

Time-resolved x-ray K -shell spectra from high density plasmas generated by ultrashort laser pulses

U. Andiel, K. Eidmann, and K. Witte

Max-Planck-Institut für Quantenoptik, D-85748 Garching, Germany

(Received 2 October 2000; published 23 January 2001)

We present time-resolved x-ray spectra of C, F, Na, and Al, generated by focusing ultrashort frequency doubled Ti:sapphire laser pulses on solid plane targets. Using a high resolution x-ray streak camera in combination with a laser triggered accumulation system, we achieved a time resolution of 1.7 ps when adding the x-ray signal of many thousands of laser shots. K -shell resonance line emission with a duration in the range of 2–4 ps is observed. Ly α emission is generally observed to be faster than He α emission and the x-ray pulse duration is observed to decrease with increasing atomic number. A hydrodynamic code in combination with an atomic kinetics code is applied for simulation of time-resolved plasma emission, showing good agreement with experimental data.

DOI: 10.1103/PhysRevE.63.026407

PACS number(s): 52.50.Jm, 52.25.Os, 32.30.Rj, 06.60.Jn

I. INTRODUCTION

Ultrashort laser pulses of subpicosecond duration focused on solid targets generate a short living hot plasma of high density. Its lifetime depends on several rapid transient processes such as the laser light absorption in the expanding plasma, the transfer of energy into the dense target, and the cooling mechanism caused by heat conduction and expansion of the plasma [1]. The progress in the performance of ultrashort pulse laser systems [2] having high repetition rates allows us to study such plasmas systematically. In particular, the emitted x rays have been a topic of growing interest during recent years [3–16]. This is motivated by the fact that the x-ray emission stems from a dense strongly coupled plasma with properties approaching those present in the interior of stars [15]. Apart from the utilization of ultrashort laser pulses, such conditions can be generated in the laboratory only in inertial confinement fusion (ICF) experiments, which require huge laser installations in contrast to the modest size of ultrashort pulse lasers. Besides this fundamental aspect, the short duration of the x-ray emission has stimulated applications for investigating ultrafast processes in matter. Here the x rays serve as a probe pulse in pump-probe experiments with the goal of reaching subpicosecond time resolution [17–19].

The recent advances in ultrafast x-ray streak cameras [20,21] has made it possible to study x-ray emission by time-resolved spectroscopy [13,14,22]. In addition, the technique of low jitter (≤ 1.7 ps) laser triggering by photoconductive switches allows the accumulation of a large number of laser shots in cases when the signal is weak [21,28]. In this paper we present time-resolved K -shell spectra from massive flat targets with low atomic number Z , consisting of C, F, Na, and Al. The experiments were performed with high contrast frequency doubled Ti-sapphire laser pulses of 150 fs duration in a modest intensity range of 10^{16} to 10^{17} W/cm². The simplicity of K -shell spectra facilitates the interpretation of the results by hydrodynamic simulations including atomic kinetics. A similar study with carbon was performed previously by Nantel *et al.* [14] but with the fundamental (not frequency doubled) Ti:sapphire radiation. In contrast to our results, which show a short emission duration of a few picose-

seconds, in Ref. [14] a long enduring emission of up to about 200 ps is reported. Time-resolved K -shell spectra from massive Al targets irradiated by longer 400 fs pulses were presented by Kieffer *et al.* [12]. Other previous work was related to measurement from targets of higher Z elements (ranging from Fe to Ta) [22], emission from preformed Al plasmas [23], and emission from very thin expanding Al foils [24].

The paper is organized as follows. In Sec. II we describe the experimental setup. The streaked spectra and the temporal pulse shapes of the main resonance lines (the Ly α and He α) and of the continuum are presented in Sec. III. In Sec. IV we compare the experimental results with hydrodynamic simulations, which were postprocessed by an atomic kinetics code.

II. EXPERIMENTAL SETUP

The experimental setup is shown in Fig. 1. The ATLAS Ti:sapphire laser system was used for plasma generation. It delivers 250 mJ laser pulses at $\lambda = 790$ Å and a pulse duration of 150 fs. The repetition rate is 10 Hz. By frequency doubling we improved the contrast ratio to 10^{10} at 2 ns and 10^6 at 1 ps before the pulse maximum. Thus preplasma formation by prepulses is avoided. The energy of the frequency doubled laser radiation ($\lambda = 395$ Å) was 80 mJ. After suppressing the fundamental radiation by a set of four selective mirrors the laser pulses were focused by an $f/3$ off axis parabolic mirror at 45° angle of incidence on solid flat targets. The focus was imaged on a charge-coupled device (CCD) camera to determine the intensity distribution [see Fig. 1(c)]. Peak values of about 5×10^{17} W/cm² are generated. In a radius of 10 μm 40% of the pulse energy is encircled, resulting in an average intensity of 7×10^{16} W/cm². By using p polarization an absorption of 40–45 % was measured at an angle of incidence of 45° [25]. The targets were disks of a few centimeters diameter, which are continuously translated and rotated to provide a fresh target surface for each laser shot. As target material we used Al, NaCl, LiF, and C (Si-gradur) with a smooth flat surface.

Time-resolved survey spectra were measured by coupling a transmission grating spectrometer to an x-ray streak cam-

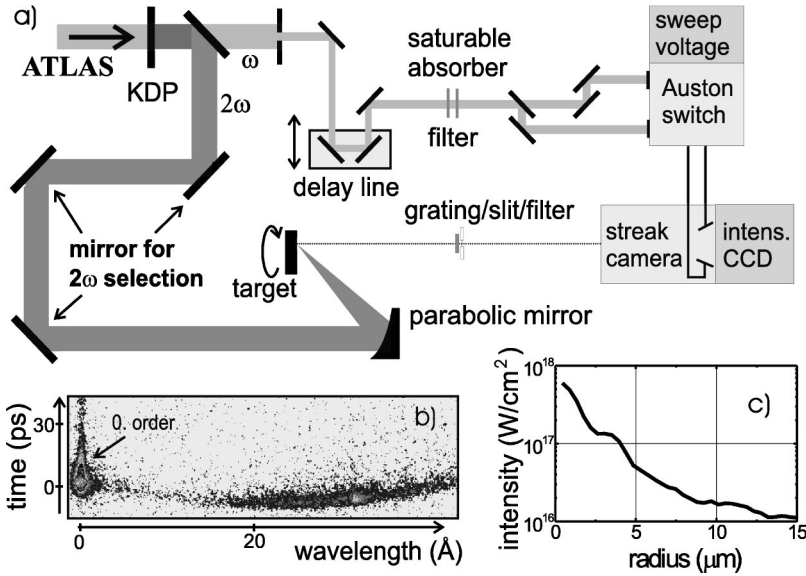


FIG. 1. (a) Experimental setup for time-resolved K -shell spectroscopy in accumulation mode. (b) Raw data of streaked carbon spectrum (accumulation of 12 000 shots). (c) Measured intensity distribution in the laser focus.

era. The transmission grating with 5000 lines per mm was mounted on a slit of $50 \mu\text{m}$ width. A thin Be filter (thickness $0.1 \mu\text{m}$) suppressed radiation at longer wavelengths, in particular in the visible range. The grating to target and grating to streak camera distances were about 56 cm. The resulting spectral resolution was $\Delta\lambda = 0.5 \text{ \AA}$.

For time resolution we used the AXIS-PX 1 streak camera [21]. Requiring small changes of the spectral sensitivity in the spectral range of interest, we chose KI cathodes for Na and F targets and KBr cathodes for Al and C targets. Both cathode materials have very narrow electron distributions in the relevant energy range [26] to provide high time resolution. In single shot operation the camera has a time resolution of 0.7 ps. However, the low collection efficiency of the spectrometer setup did not allow for single shot operation. For this reason we accumulated up to 12 000 laser shots by installing a laser triggered semiconductor switch (a so-called Auston switch) [27], thereby achieving a high signal to noise ratio of the detected spectra. We used about 0.5 mJ of the fundamental laser pulse energy to illuminate two photoconductive GaAs switches for triggering the sweep voltage on the deflection plates of the streak camera with high temporal stability [28]. A remaining small temporal jitter is still generated by fluctuations of the amplified spontaneous emission (ASE) pedestal preceding the laser pulses of the ATLAS system. This leads to small fluctuations of the sweep voltage due to premature discharge of the semiconducting switches. By using a saturable absorber in front of the switches, we suppressed the ASE level substantially and managed to end up with a time resolution of 1.7 ps in accumulation mode of the streak camera, even when we accumulated up to 10 000 shots [28]. The time resolution of 1.7 ps obtained by us is an outstanding value for Ti:sapphire laser systems with a repetition rate of 10 Hz which to our knowledge was not achieved previously (compare Ref. [14], where a time resolution of 4 ps was obtained).

An example of a raw spectrum is depicted in Fig. 1(b) for carbon as target material. The curvature of the streaked spectrum is caused by different electron paths, which are shortest

for electrons emitted at the center of the slit and increase for electrons emitted at some distance from the center.

III. EXPERIMENTAL RESULTS

In our analysis the raw data were corrected for the curvature as well as for the spectral sensitivity of the photocathode. Resulting streaks for the different materials are presented in Fig. 2.

The plotted spectra (solid lines) are obtained by integrating the streaked spectra over a time approximately corresponding to the line duration. As dominating lines we observe the $2p-1s$ ($\text{Ly } \alpha$) and $1s2p-1s^2$ ($\text{He } \alpha$) transitions. The ratio of $\text{Ly } \alpha$ to $\text{He } \alpha$ intensity decreases with Z . This is expected because in lower Z plasmas the hydrogenlike ions have a lower ionization energy and are therefore more easily ionized. The $\text{Ly } \alpha$ line of Al can no longer be identified. This is in agreement with previous time-integrated Al spectra measured with high spectral resolution by means of a von Hamos crystal spectrometer [15,16]. These measurements showed that the $\text{Ly } \alpha$ intensity was lower than the $\text{He } \alpha$ intensity by a factor of 10. The $\text{He } \alpha$ line of F and the $\text{Ly } \alpha$ line of C are clearly broader than the spectral resolution ($\Delta\lambda = 0.5 \text{ \AA}$). Their long wavelength wing is less steep than the short wavelength wing. Time-integrated but spectrally highly resolved Al spectra, which were previously measured under the same conditions [15,16], indicate that this spectral line shape is caused by merging of the resonance line with its satellites in the presence of strong electron Stark broadening due to the high density of the plasma.

Temporal lineouts are taken by spectrally averaging over the full line profiles, including their poorly resolved satellite emission. The time history of the resonance lines taken from the streaked spectra is shown in Fig. 3. In some cases [see, for example, the $\text{Ly } \alpha$ line of carbon in Fig. 3(a)] the time profiles show asymmetric shapes. A steep rise is followed by a slower decay. We notice that the response of the streak camera is still included in these data. For quantitative evalu-

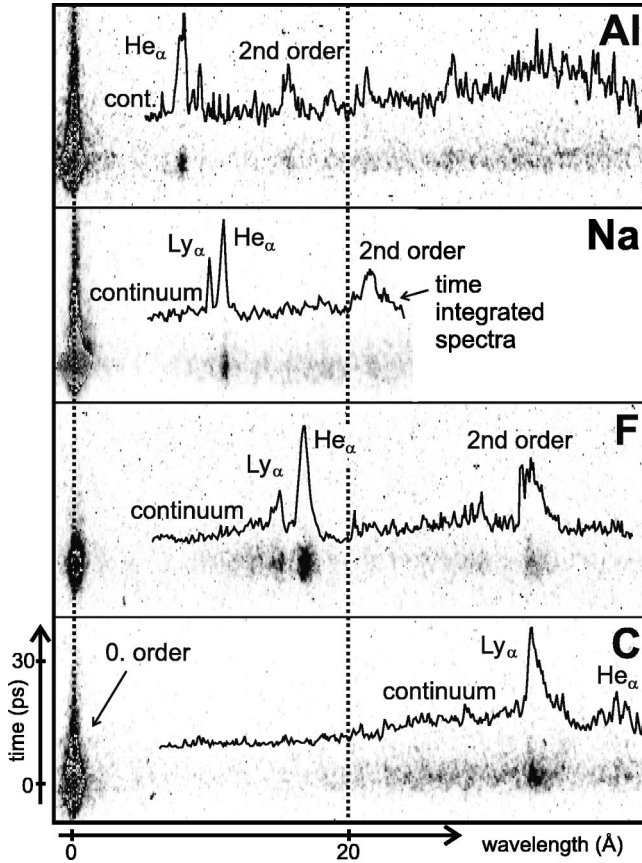


FIG. 2. Experimental data for different target materials. Streaks are corrected for curvature and spectral sensitivity of the photocathodes. Time-integrated lineouts are plotted as solid lines.

ation, we unfolded the time-resolved measurements by using the formula

$$\Delta t_{\text{unfolded}} = \sqrt{\Delta t_{\text{measured}}^2 - \Delta t_{\text{res}}^2},$$

where $\Delta t_{\text{res}} = 1.7$ ps is the resolution of the x-ray streak camera in accumulation mode. The unfolded duration [full width at half maximum (FWHM)] of the observed resonance lines is presented in Fig. 4 as a function of the atomic number Z . The duration of both the He α and the Ly α emission decreases with Z . Also, the Ly α emission is shorter than the He α emission. Thus, the larger the ionization or excitation energies, the shorter the emission. Qualitatively, this behavior is related to the fact that the higher ionization or excitation energies require a hotter plasma, which is expected to have a shorter lifetime, as will be discussed in the next section.

We also analyzed the spectral characteristics of the bound-free continuum, which is indicated in Fig. 2 on the high energy side of the resonance lines. To show the continuum more clearly, we have plotted the spectrum semilogarithmically in Fig. 5(a) in the case of carbon. The slope of the continuum can be well fitted by the exponential Boltzmann expression [$\propto \exp(-h\nu/kT)$]. The temperature obtained from such a fit increases with the atomic number. We find 110 eV for carbon [Fig. 5(a)], 200 eV for fluorine, 280 eV

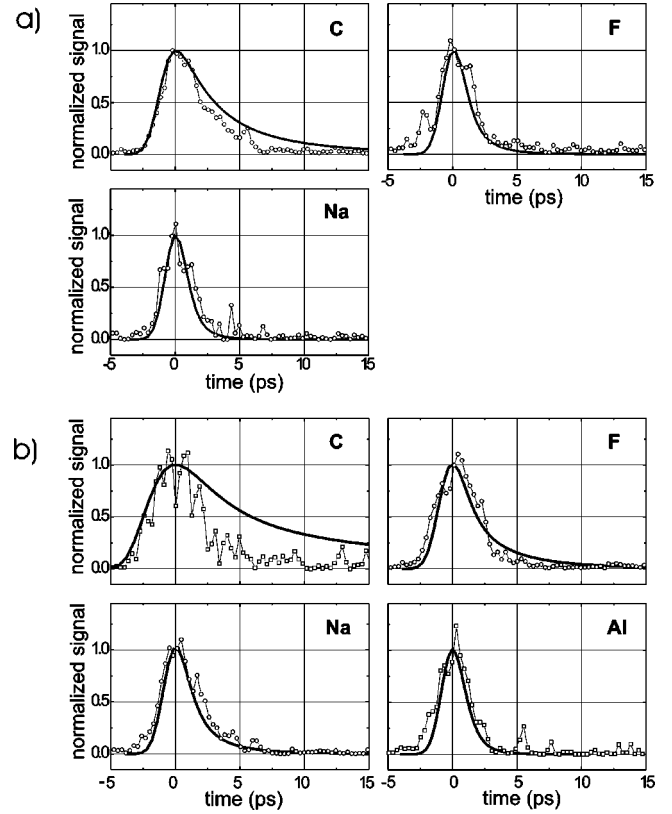


FIG. 3. Time profiles of Ly α (a) and He α (b) emission for different materials. Experimental data are compared to hydrodynamic code simulation (full lines).

for sodium, and about 300 eV for aluminum. The temperature for aluminum is in reasonable agreement with electron temperatures deduced from spectral analysis in previous experiments [32].

In the case of the carbon continuum emission, we also performed a temporal analysis. The temporal lineout was taken as a spectral average over the region 25 to 29 Å (or 430 to 500 eV) and is plotted in Fig. 5(b). After unfolding the streak camera response, a FWHM duration of 3.2 ps is determined from the measurement. This value is very close to the carbon resonance line duration plotted in Fig. 4.

IV. COMPARISON WITH NUMERICAL SIMULATIONS

Simulations are performed with the MULTI-fs hydrodynamic code [1]. It is based on the MULTI code [29], which is

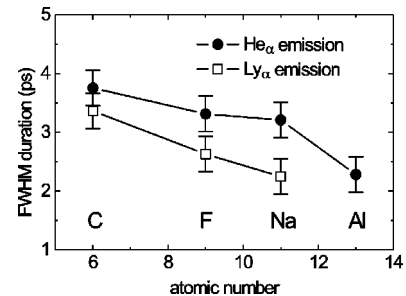


FIG. 4. FWHM duration (after unfolding with the time resolution of the streak camera) for different target elements.

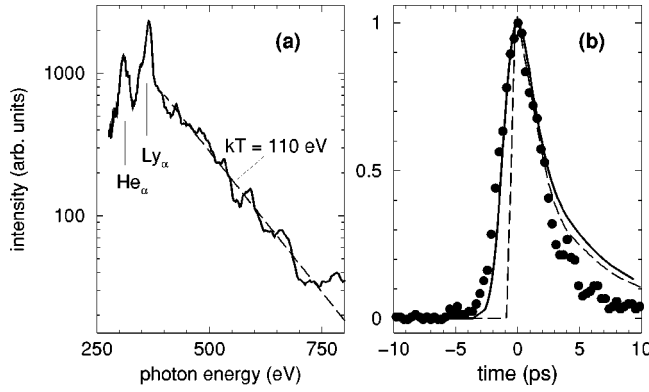


FIG. 5. (a) Bound-free continuum of carbon. The data are time integrated over the duration of the emission. The dashed line is the Boltzmann fit used for temperature determination. (b) Temporal lineout of bound-free continuum (dots). Experimental data are compared with hydrodynamic code simulation. The simulation result is plotted as the dashed line and after convolution with the experimental response function as the solid line.

a Lagrangian code developed for nanosecond laser pulse interaction with solid targets. MULTI-fs is adapted to subpicosecond laser pulses by solving Maxwell's equations in a steep density gradient plasma. The nonequilibrium between electrons and ions is taken into account. Also, a model for electrical and thermal conductivity is included, which can be applied from solid state to high temperature plasma. The electronic heat transport is described by Spitzer's heat conductivity. The heat flux is limited by the free-streaming limit, i.e., the so-called f factor is set to $f=0.6$, which corresponds to a Maxwellian electron distribution [30]. The hydrodynamic simulations are performed in one-dimensional plane geometry. For the time dependence of the laser pulse we assumed a squared sinusoidal function [$S_L(t) \propto \sin^2(\pi t/2\tau)$ with $\tau=150$ fs].

MULTI-fs calculates the electron temperature and density in each Lagrangian cell as a function of time for a given laser intensity. In Fig. 6 temperature and density profiles are shown for an Al target at different times as a function of the spatial coordinate x . The initial target surface is located at $x=0$. The absorbed intensity in this simulation corresponds to the experimentally determined absorbed intensity of 3×10^{16} W/cm² (average over 10 μ m focal radius). As in the experiment, the incident laser light is p polarized at an angle of incidence of 45°. The ablated material expands into the vacuum. In the expanding plasma, the laser pulse is absorbed, heating the low density plasma up to several keV. Due to the process of resonance absorption, the laser energy deposition occurs preferentially at the critical density $\rho_{cr} = 0.025$ g/cm³ (corresponding to $n_{cr} = 7.2 \times 10^{21}$ cm⁻³). The hot electrons created at the critical layer penetrate into the dense target and generate a diffusive heat wave with a rather homogeneous temperature profile at densities close to solid state. The simulation demonstrates the penetration of the heat wave into the target material, while the average temperature is rapidly decreasing on a picosecond time scale. Within 5 ps the heat wave has propagated more than 500 nm into the target, still heating the electrons in this volume up to about

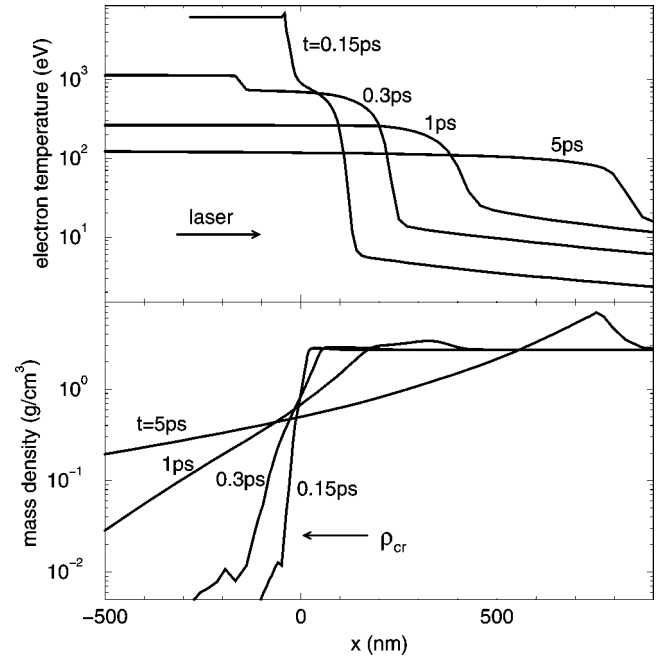


FIG. 6. Electron temperature and density for different times as a function of the layer depth x for an Al target at an absorbed intensity of 3×10^{16} W/cm². The cold target surface corresponds to $x=0$. The penetration of a thermal wave into the target is illustrated.

100 eV. After a few picoseconds, a shock wave builds up that is driven by the high pressure generated by the ablating matter.

In our relevant intensity range, greater than 10^{16} W/cm², the hydrodynamic model approaches its limits, because the electron mean free path starts to exceed the scale length of the expanding low density plasma in the region of the critical layer. This causes nonlocal heat transport, not taken into account by MULTI-fs, which uses a local temperature. Nevertheless, in the dense region of the target the penetrating electrons thermalize quickly because their mean free path is reduced strongly and is still small enough for the development of a diffusive heat wave. This is confirmed by collisional particle-in-cell simulation [31] and other experiments [32]. Since our analysis shows that the emitted radiation is mainly generated in the dense diffusively heated target region, we believe that the applied hydrodynamic code is still a reasonable approximation for our conditions.

We also note that MULTI-fs neglects density profile modifications due to the light pressure. This may slightly modify the density initially during the interaction with the laser [33]. Since the duration of the laser pulse of 150 fs is much shorter than the duration of the x-ray emission, we believe that modifications due to the light pressure are not very important for our conditions.

To calculate the K -shell emission, the hydrodynamic results of MULTI-fs have been postprocessed by means of the atomic kinetics code FLY [35–37]. A similar procedure of postprocessing has been applied previously [34]. It is noted that MULTI-fs takes into account radiation emission and transport; however, in a steady state approximation by using opacity tables [1]. Since the x-ray generation is only a small

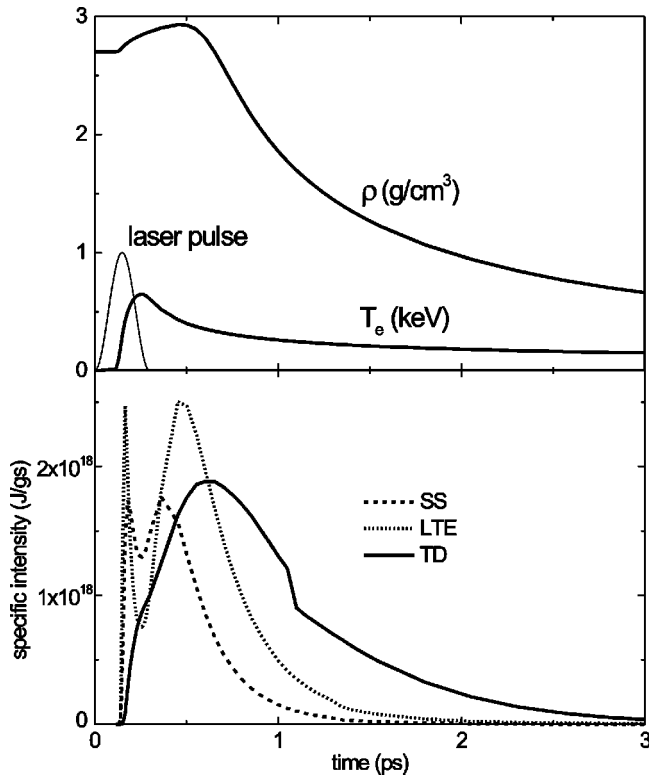


FIG. 7. Top: time history of the density and temperature for a layer at a depth of 90 nm (at $t=0$). Laser parameter and target are as in Fig. 6. Bottom: time history of the Al He α emission calculated with the FLY code under the assumption of steady state (SS), local thermal equilibrium (LTE), and by solving the time-dependent rate equations (TD).

contribution (typically less than 1%) in the energy balance, one can assume that the hydrodynamic behavior is not much influenced by details of the radiation emission and transport. This justifies our procedure of postprocessing.

The FLY code solves the rate equations for the different populations. As input it uses the time history of the density and temperature of the Lagrangian layers. Figure 7 shows an example of one layer of an Al target, at the depth 90 nm (or 2.4 g/cm²), from which depth the major contribution is emitted during the first picosecond. At the top of Fig. 7 the time histories of the density and temperature are plotted. After a short delay the heat wave has reached the considered layer and the temperature rises up to 600 eV at the end of the laser pulse. Then it drops slowly during the next few picoseconds. The density is first slightly enhanced due to compression. Then after ≈ 0.5 ps expansion sets in. At the bottom, Fig. 7 shows the specific emission of the He α line. To illustrate the importance of the transient effect, we compare results of the time-dependent solution of the rate equations (TD) with results obtained under the assumption of steady state (SS) and of local thermal equilibrium (LTE). It is seen that the time-dependent result differs strongly from SS or LTE results. Both LTE and SS overestimate the onset of emission, while overionization causes a gap in the emission signal at early times. In contrast, the time-dependent calculation gives a smoother onset of the emission and a longer tail, resulting in

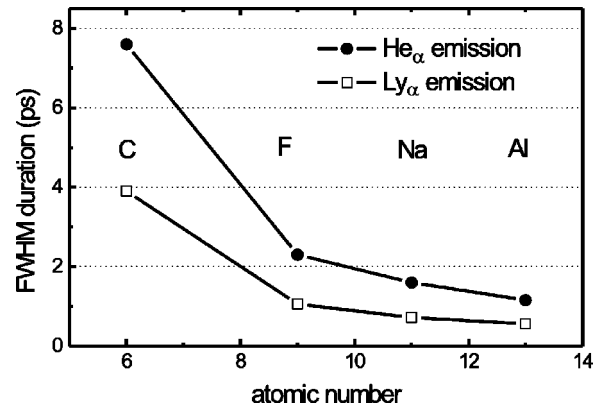


FIG. 8. The FWHM duration of simulated Ly α and He α emission from different target materials. The trend of decreasing pulse duration with growing atomic number is consistent with the experiment (Fig. 4).

a longer emission time, which is closer to the experimental observation.

To obtain the total x-ray emission one has to sum over the emission from all layers. The results obtained for the FWHM pulse durations of He α and Ly α lines are shown in Fig. 8 for the different materials used in the experiment. For a direct comparison with experimental data, we also plotted the x-ray pulses after convolution with the experimental streak camera resolution ($\Delta_{res} = 1.7$ ps) in Fig. 3 (solid lines).

The calculated pulse durations (Fig. 8) show the same trend as the experiment (Fig. 4). They decrease with the atomic number and Ly α emission is generally shorter than He α emission. The absolute pulse durations somewhat differ from the experimental data. The calculated durations of the carbon lines are overestimated, while for the larger Z elements (Na and Al) the theoretical pulses are somewhat shorter than the experimental ones. One reason for these deviations may be the fixed intensity chosen for simplicity in the simulations for all elements. Increasing the laser intensity results in longer x-ray pulse durations as shown in Fig. 9 in the case of the Al He α . Experimental data can therefore be better reproduced when using a lower intensity for carbon and higher intensities for the larger Z materials. This is consistent with the fact that a higher average laser intensity is

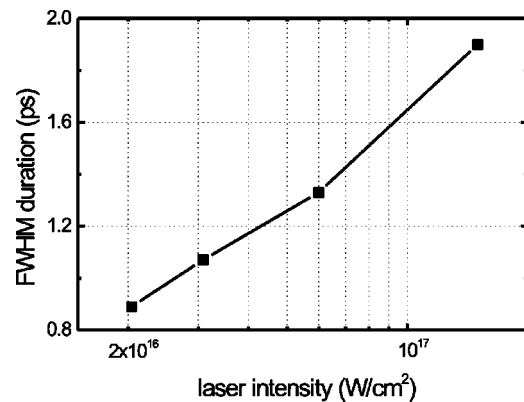


FIG. 9. Simulation results for Al He α FWHM pulse duration as a function of the absorbed laser intensity.

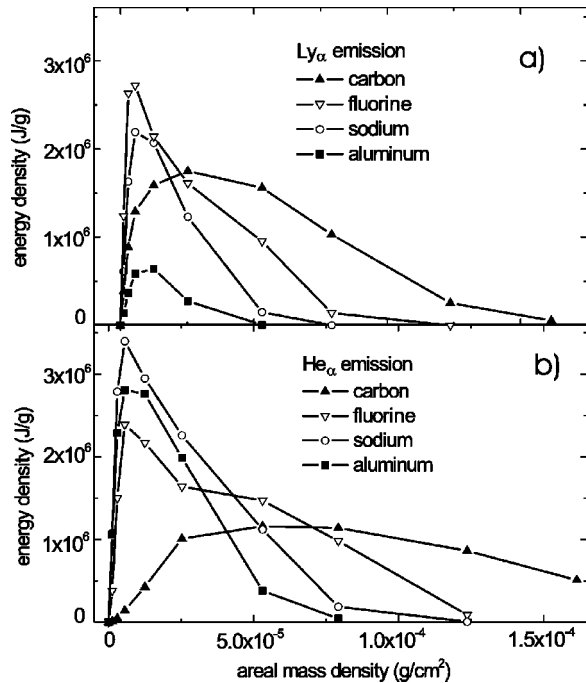


FIG. 10. Time-integrated emitted energy per mass as a function of the areal mass density for Ly α (a) and He α (b) line emission. The emitting region grows with decreasing atomic number of the target material and emission contributions of layers deep inside the target are no longer negligible.

needed for elements with larger Z to create K -shell emission, because the excitation and ionization energies increase with increasing Z . Considering the focal intensity distribution in the experiment [see Fig. 1(c)], the emitting spot size is therefore expected to decrease with increasing Z . This is confirmed by the fact that the temperature found from the continuum increases with increasing atomic number. Also, in a previous experiment it was found that the radius of the spot size of the x-ray emission from a gold target increased with the x-ray wavelength from about $5 \mu\text{m}$ at $\approx 5 \text{ \AA}$ to $20 \mu\text{m}$ radius at $\approx 40 \text{ \AA}$ [32]. This experimental result indicates that the average intensity of the softer x-ray emission is lower than for the harder x rays.

Another reason for the discrepancies in the pulse duration between the experiment and the calculation may be the neglect of opacity effects when we did the summation over the contributions from the different layers. To illustrate the spatial origin of the line emission, we plotted, in Fig. 10, the time-integrated specific energy of resonance line emission over the areal mass density for different target materials. For aluminum, the emission stems mainly from a thin surface layer of about $4 \times 10^{-5} \text{ g cm}^{-2}$ (corresponding to a 150 nm thick surface layer in the solid state). The electron temperature in deeper layers is not high enough for aluminum K -shell emission to be generated. For target materials with lower atomic number, deeper layers contribute more efficiently and the radiating depth is substantially increased. The increase of the calculated line duration for decreasing atomic number (Fig. 6) can be attributed to the fact that the emission from deep layers is delayed compared to the radiation from

less deep layers due to the propagation time of the thermal heat wave into the target.

Considering the broad emitting volume deep inside the carbon target material [see Fig. 10(b)], opacity may influence the time history of the emitted lines. In particular, the rather large discrepancy of the carbon He α line duration between experiment and simulation may be attributed to opacity effects. Emission from deep layers can be efficiently absorbed in this case on its way to the target surface. Since this emission is generated at delayed times compared to the radiation from front layers, opacity will finally shorten the detectable pulse duration in the experiment. The simulated duration of x-ray emission should therefore be considered as a maximum value in the case of low Z target materials, since opacity effects were not included in our model.

In contrast to the resonance line emission, continuum radiation has the advantage that opacity effects are not important. The time history of the bound-free continuum emission observed in the experiment was modeled for carbon as the target material. The result is plotted in Fig. 5(b). The simulation shows good agreement with the experimental data.

V. SUMMARY AND CONCLUSIONS

K -shell spectra from different low and medium Z materials irradiated with ultrashort laser pulses are presented. The spectra were detected in accumulation mode at 1.7 ps time resolution by means of an Auston switch triggering system.

The pulse durations of the resonance lines are in the range of a few picoseconds. Hydrogenlike resonance lines show shorter pulse durations compared to heliumlike lines for all elements, while the durations generally decreasing with increasing atomic number.

Hydrodynamic code simulations postprocessed with an atomic kinetics code agree well with the experimental results. The remaining discrepancies are discussed and can be attributed to intensity and opacity effects. In contrast to the resonance line radiation, the plasma is optically thin for the bound-free continuum, which shows good agreement with the theoretical modeling.

A very important result of our model is that the emission under our conditions stems mainly from the dense target, which is heated isochorically by electron heat conduction while the emission from the very hot expanding low density front plasma is negligible. This is in agreement with our previous analysis of time-integrated Al spectra, which indicated high densities close to the solid state at temperatures of 250 to 300 eV [15,16].

ACKNOWLEDGMENTS

The authors are very grateful to J. Bayerl for setup constructions and A. Böswald and H. Haas for operating the laser system. This work was supported in part by the European Communities within the framework of the Euratom-IPP association and by the Deutsche Forschungsgemeinschaft in the framework of the Schwerpunktsprogramm ‘‘Wechselwirkung intensiver Laserfelder mit Materie.’’

- [1] K. Eidmann, J. Meyer-ter-Vehn, and T. Schlegel, *Phys. Rev. E* **62**, 1202 (2000).
- [2] D. Strickland and G. Mourou, *Opt. Commun.* **56**, 219 (1985).
- [3] O.L. Landen, E.M. Campbell, and M.D. Perry, *Opt. Commun.* **63**, 253 (1987).
- [4] A. Zigler, P.G. Burkhalter, D.J. Nagel, M.D. Rosen, K. Boyer, T.S. Luk, A. McPherson, and C.K. Rhodes, *Opt. Lett.* **16**, 1261 (1991).
- [5] M.M. Murnane, H.C. Kapteyn, M.D. Rosen, and R.W. Falcone, *Science* **251**, 531 (1991).
- [6] G.A. Kyrala, R.D. Fulton, E.K. Wahlin, L.A. Jones, G.T. Schappert, J.A. Cobble, and A.J. Taylor, *Appl. Phys. Lett.* **60**, 2195 (1992).
- [7] P. Audebert, J.P. Geindre, J.C. Gauthier, A. Mysyrowicz, J.P. Chambaret, and A. Antonetti, *Europhys. Lett.* **19**, 189 (1992).
- [8] U. Teubner, J. Bergmann, B. von Wonterghem, and F.P. Schäfer, *Phys. Rev. Lett.* **70**, 794 (1993).
- [9] J.C. Kieffer, M. Chaker, J.P. Matte, H. Pépin, C.Y. Côté, Y. Beaudoin, T.W. Johnson, T.W. Chien, T.W. Coe, G. Mourou, and O. Peyrusse, *Phys. Fluids B* **5**, 2676 (1993).
- [10] J. Workman, A. Maksimchuk, X. Liu, U. Ellenberger, J.S. Coe, C.Y. Chien, and D. Umstadter, *Phys. Rev. Lett.* **75**, 2324 (1995).
- [11] Z. Jiang, J.C. Kieffer, J.P. Matte, M. Chaker, O. Peyrusse, G. Gilles, G. Korn, A. Maksimchuk, S. Coe, and G. Mourou, *Phys. Plasmas* **2**, 1702 (1995).
- [12] J.C. Kieffer, Z. Jiang, A. Ikhlef, and C.Y. Côté, *J. Opt. Soc. Am. B* **13**, 132 (1996).
- [13] P. Gallant, Z. Jiang, J. Fuchs, J.C. Kieffer, H. Pépin, D. Gontier, A. Mens, N. Blanchot, J.L. Miquel, J.F. Telletier, and M. Sutton, *Proc. SPIE* **3157**, 44 (1997).
- [14] M. Nantel, G. Ma, S. Gu, C.Y. Côté, J. Itatani, and D. Umstadter, *Phys. Rev. Lett.* **80**, 4442 (1998).
- [15] A. Saemann, K. Eidmann, I.E. Golovkin, R.C. Mancini, E. Andersson, E. Förster, and K. Witte, *Phys. Rev. Lett.* **82**, 4843 (1999).
- [16] K. Eidmann, A. Saemann, U. Andiel, I.E. Golovkin, R.C. Mancini, E. Andersson, and E. Förster, *J. Quant. Spectrosc. Radiat. Transf.* **65**, 173 (2000).
- [17] F. Raksi, A. Ikhlev, C.Y. Côté, and J.C. Kieffer, *J. Chem. Phys.* **104**, 6066 (1996).
- [18] C. Rischel, A. Rousse, I. Uschmann, P.A. Albouy, J.P. Geindre, P. Audebert, J.C. Gauthier, E. Förster, J.L. Martin, and A. Antonetti, *Nature (London)* **390**, 490 (1997).
- [19] C.W. Siders, A. Cavalleri, K. Sokolowski-Tinten, C. Toth, T. Guo, M. Kammler, M. Horn von Hoegen, K.R. Wilson, D. von der Linde, and C.P.J. Barty, *Science* **286**, 1340 (1999).
- [20] R. Shepherd, R. Booth, D. Price, M. Bowers, D. Swan, J. Bonlie, B. Young, J. Dunn, B. White, and R. Steward, *Rev. Sci. Instrum.* **66**, 719 (1995).
- [21] C.Y. Côté, J.C. Kieffer, P. Gallant, J.C. Rebuffie, C. Goulmy, A. Maksimchuk, G. Mourou, D. Kaplan, and M. Bouvier, *Proc. SPIE* **2869**, 956 (1997).
- [22] J.F. Pelletier, M. Chaker, and J.C. Kieffer, *Appl. Phys. Lett.* **69**, 2172 (1996).
- [23] C.Y. Côté, J.C. Kieffer, and O. Peyrusse, *Phys. Rev. E* **56**, 992 (1997).
- [24] P. Gallant, Z. Jiang, C.Y. Chien, P. Forget, F. Dorchies, J.C. Kieffer, H. Pepin, O. Peyrusse, G. Mourou, and A. Krol, *J. Quant. Spectrosc. Radiat. Transf.* **65**, 243 (2000).
- [25] R. Rix, Diplomarbeit, Universität Erlangen, 1999.
- [26] B.L. Henke, J. Liesegang, and S.S. Smith, *Phys. Rev. B* **19**, 3004 (1979).
- [27] W. Knox and G. Mourou, *Opt. Commun.* **37**, 203 (1981).
- [28] C.Y. Côté, D. Kaplan, M. Bouvier, K. Eidmann, J. Tesar, and J.C. Kieffer, *Proc. SPIE* **3414**, 280 (1998).
- [29] R. Ramis, R. Schmalz, and J. Meyer-ter-Vehn, *Comput. Phys. Commun.* **49**, 475 (1988).
- [30] W.L. Kruer, *The Physics of Laser Plasma Interactions* (Addison-Wesley, New York, 1988).
- [31] R.E.W. Pfund, Dissertation, Technische Universität München, 1999.
- [32] A. Saemann, Dissertation, Technische Universität Darmstadt, 1998.
- [33] O. Peyrusse, M. Busquet, J.C. Kieffer, Z. Jiang, and C.Y. Côté, *Phys. Rev. Lett.* **75**, 3862 (1995).
- [34] K. Eidmann and F. Pisani, in *Laser Interaction with Matter and Inertial Fusion*, edited by G. Velarde *et al.* (World Scientific, Singapore, 1997), p. 465.
- [35] R.W. Lee, B.L. Whitten, and R.E. Strout, *J. Quant. Spectrosc. Radiat. Transf.* **32**, 91 (1984).
- [36] R.W. Lee, *J. Quant. Spectrosc. Radiat. Transf.* **40**, 561 (1988).
- [37] R.W. Lee and J.T. Larson, *J. Quant. Spectrosc. Radiat. Transf.* **56**, 535 (1996).